Radiative heating of inertial particles in a particle-laden turbulent duct flow

Laura Villafañe[1*], Andrew Banko[1], Ji Hoon Kim[1], Chris Elkins[1], John K. Eaton[1]

1: Department of Mechanical Engineering
Stanford University
Stanford, CA 94305
*Corresponding author: lvillafa@stanford.edu

ABSTRACT

Radiation absorption by disperse solid particles in a turbulent square duct flow was studied experimentally for different particle loadings. The fully-developed flow of air at a Reynolds number of $\mathrm{Re_H} = 20 \cdot 10^3$ was loaded with 12 μm diameter Nickel particles and exposed to monochromatic near-infrared radiation. Optical measurements confirmed the existence of significant preferential concentration at the low loadings. Total radiation transmission through the particle laden flow and mean gas temperature rise, were analyzed for mass loading ratios ranging from 0.1 to 0.4. Transmission measurements are in good agreement with the exponential decay predicted by the Beer-Lambert law. Estimates of the gas temperature rise from a one-dimensional model making use of the optically thin approximation are found to over predict the gas temperature at the highest loading when compared with the experimental data.

INTRODUCTION

The interaction of disperse, heavy particles in a turbulent flow is well studied due to wide interest in the phenomena of preferential concentration (Maxey, 1987; Squires & Eaton, 1991). This interest stems from the large number of systems in which heavy particles are transported in a background turbulent flow, and the impact that particle number density fluctuations may have in the overall system behavior. A classic example is droplet collisions in clouds, which is thought to be enhanced by preferential concentration (Sundaram & Collins, 1997). In spray and coal combustion, slurry catalysis, and enhanced heat transfer fluids, the disperse phase acts as localized sources of heat and mass transfer in a background flow that is typically turbulent for Reynolds numbers of industrial interest (Williams, 1958; Brian *et al.*, 1969; Kuerten *et al.*, 2011). As a result, number density fluctuations can lead to increased inhomogeneities in the local thermodynamic state. In addition, statistical correlations in particle positions are known to impact radiation transfer through, and radar reflection from, clouds (Shaw *et al.*, 2002; Matsuda *et al.*, 2014).

Particle-based solar receivers pose an interesting engineering challenge because many of the processes listed above are simultaneously present. Volumetric absorption by a working fluid seeded with small particles minimizes the energy losses due to surface reradiation that penalizes conventional surface absorbers (Lenert & Wang, 2012). The use of particle-based solar receivers for gas heating in various applications was examined by different researchers experimentally (Klein *et al.*, 2008; Kim *et al.*, 2009; Bertocchi *et al.*, 2004) and numerically (Miller & Koenigsdorff, 2000; Chen *et al.*, 2007; Crocker & Miller, 2011). However those studies neglected the effects of carrier phase turbulence.

Depending on the particle size, material, volume fraction, and carrier phase properties, coupling between radiation, particle distribution, and background turbulence can lead to modified system efficiencies. The exchange of momentum between a turbulent fluid and particles is responsible for the dynamic formation of preferential concentration and the modulation of the turbulent field (Fessler *et al.*, 1994). In the presence of an external source of radiation, the existence of large voids and partially shadowed particles can reduce the total amount of radiation absorbed (Matsuda *et al.*, 2012). Note that we consider the fluid (gas or liquid) to be transparent to radiation, and the particles to be the absorbing agent. The thermal energy absorbed in high particle concentration regions is transferred to the surrounding gas. Thus, preferential concentration induces local hot spots which can impact the performance of downstream power generation components (Yapa *et al.*, 2015). If the energy input from radiation is large enough, the variable density gas may expand and local sources of buoyancy may also alter the background turbulence leading to the redistribution of particles in the flow (Zamansky *et al.*, 2014). Pouransari & Mani (2017) and Rahmani *et al.* (2015) showed that turbulence-particle interactions inducing preferential concentration can have a significant impact on the output particle temperatures while having little effect on the mean gas temperature. However those studies assumed the medium to be optically transparent ignoring the effect of particle shadowing or radiation attenuation, and did not account for real effects in practical applications such as the presence of walls, or turbophoresis (Reeks, 1983). Works exploring the complete physics of particle-turbulence-radiation interaction are scarce. In addition, little experimental data exists that can be used for model validation or for providing evidence on the extent to which preferential concentration impacts radiation absorption and transmission in multiphase flows.

We present an experimental study in which a fully-developed particle-laden turbulent flow in a square duct is exposed to monochromatic near-infrared radiation. The flow regime and particle characteristics chosen are such that particle-turbulence interactions induce large fluctuations in particle concentration. A detailed analysis of the particle concentration fluctuations measured in the absence of radiation is given in Villafañe *et al.* (2017). In regard to the particle phase, we concentrate in the mean particle velocity and concentration that determine the amount of particles exposed to the incident radiation and their exposure time. The convective heating of the turbulent phase by the energy absorbing particles is evaluated from gas temperature measurements for different conditions of particle loading. In addition, integral measurements of total transmitted radiation serve to study the radiation attenuation for varying particle loading. We make use of a one-dimensional heat transfer model to understand the effect of the particle, flow and radiation parameters on the gas temperature at the center of the duct. The temperature rise predicted by the model and estimated values of total transmission through the mixture are compared to the experimental measurements. This comparison shows the importance of coupling effects ignored in simplified models.

EXPERIMENTAL METHODS

The experiments were performed in a fully-developed, vertical, turbulent square duct flow facility at Stanford University. The open loop wind tunnel and the test section are pictorially described

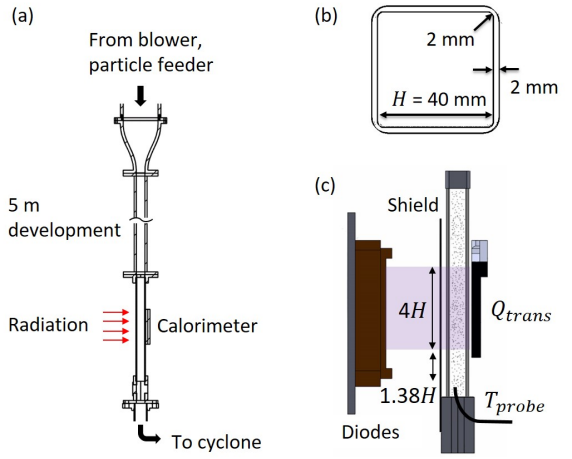

Figure 1. Experimental apparatus: (a) Flow conditioning, development length, and test section, (b) test section cross-section, (c) diode array, calorimeter, and thermocouple probe location.

in Fig.1. All the flow, particle and radiation measurements are performed in the test section. For a detailed description of the facility and its characterization see Villafañe *et al.* (2017). The main flow of air is driven by a variable speed centrifugal pressure blower. A closed loop controller, regulates the blower to ensure a constant test section Reynolds number, which is defined based on the duct width, bulk velocity and kinematic air viscosity at the test section.

Particles are injected by a volumetric screw feeder into a flow conditioning section where they are dispersed laterally by several grids. The particle-air mixture is accelerated through a 16:1 contraction as it enters the flow development section. A 5.4 m-long smooth aluminum duct with a 40 mm-wide internal square cross section ensures that by the time the gas-particle mixture reaches the test section the flow is fully-developed, and the particles are independent of the manner in which they were injected (Lau & Nathan, 2014). The test section is a 425 mm long duct made of borosilicate glass, with a wall thickness of 2 mm, and a nominal internal square cross-section of 40 mm $\times$ 40 mm. The cross-section deviates from a perfect square due to the the presence of 2 mm internal corner radii, as indicated in Fig. 1b. This internal curvature is a consequence of the requirement of fabricating the test section as a continuous glass piece to eliminate joints, that would constitute regions of high radiation absorption. After being exposed to radiation in the test section, the mixture passes through a cyclone separator where the particles are collected for re-use.

The radiation source is a high power laser diode array manufactured by Princeton Optronics Inc. that provides near collimated radiation at a wavelength of 975 nm. The output beam from the diodes is masked to illuminate the full width of the duct for a streamwise length of 160 mm, or four duct widths, as sketched in Fig. 1c.

All experiments in this study were performed at a Reynolds number of $\mathrm{Re_H} = 20,000$, with a 0.75% uncertainty. The nickel particles used are nearly spherical with a number based mean diameter of 11.8 +/- 0.5 microns. Particle size distributions measured with a Coulter Counter showed a relatively narrow distribution with low probability tails that cover a range from about 6 to 20 μm. Comparison of particle probability size distributions before and after an experiment demonstrated that particle sizes are not selectively filtered by the rig and downstream cyclone separator. The extent to which particles preferentially concentrate is mainly dictated by the Stokes number, St_η, that represents the ability of particles to follow the turbulent fluctuations in the flow. The Stokes number is defined as the ratio of the particle aerodynamic relaxation time to the Kolmogorov time scale of the turbulence, computed using a channel averaged dissipation rate. At the flow conditions tested, the averaged Stokes number is $\overline{St_\eta} = 12$. Experiments were performed at different mass loading ratios, Φ, defined as the ratio of the mass flow rate of particles to the mass flow rate of air. Loadings were varied from $\Phi = 0.025$ to 0.4, with an uncertainty of about 0.004 in the mean value. Despite the moderate loadings, the particle volume fraction remained under $O(10^{-4})$. The test section was exposed to 1 kW $\pm$ 2% incident radiation. The 2 mm thick borosilicate walls were measured to be about 91% transmissive for the particular wavelength used, leaving the gas-particle mixture nominally exposed to about 910 W.

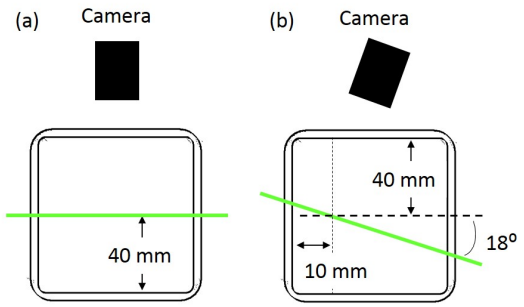

Figure 2. Laser sheet configurations for PIV and concentration measurements (a), and for near-wall mean concentration (b).

Optical measurements of the particle-phase velocity and concentration were made in the absence of heating to evaluate the radiated section inlet conditions. Two-dimensional Particle Image Velocimetry (PIV) techniques were used to obtain mean streamwise particle velocities at the central test section plane from 2000 image pairs. The uncertainty on the mean velocities is less 0.3%. Measurements of particle concentration used two-dimensional coordinates of particle centroids derived from the same dataset using one of the images from each PIV pair. A complete description of the imaging techniques is given in Villafañe *et al.* (2017). Villafañe *et al.* (2016) discusses the methods used to quantify preferential concentration. The field of view is limited in the wall normal direction by the curved test section corners. In order to measure the concentration distribution near to the wall an angled laser sheet configuration was adopted. Figure 2 shows the laser sheet configurations for the wall perpendicular and angled cases.

Total transmitted power and mean gas temperature rise were measured. A water cooled copper calorimeter with a black painted surface facing the radiation source at the opposite side of the test section provided the total transmitted power. The uncertainty in the transmitted power is about $\pm$ 10 W accounting for the uncertainty in the cooling water flow-rate and the water temperature rise across the calorimeter. The mean gas temperature rise in the gas was measured with a custom 75 micron diameter butt-welded K-type thermocouple probe with wires perpendicular to the flow direction and a half length of about 2.5 mm. It is mounted on an L-shaped stem to avoid flow disturbances at the measurement location. The probe was traversed along the wall bisector from the center point of the duct towards the test section wall closest to the radiation system, at 55 mm below the radiated section. This distance is required to avoid errors due to scattered radiation absorbed by the thermocouple. The estimated uncertainty in the temperature rise measurement is 0.2^oC.

RESULTS

The gas temperature rise is first analyzed using a simplified one-dimensional model that allows a clear interpretation of the in-

fluence of the system parameters on gas and particle temperature evolution along the radiated section. We then present results for the particle-phase velocity and distribution across the test section in the wall normal direction, gas temperature profiles, and total radiation attenuation. Particle-turbulence-radiation interactions usually occur in a confined flow, which posses the added complexities of shear, turbophoresis and wall heat transfer. To evaluate the effect of those added complexities the experimental data are contrasted to the predicted temperature rise from the one-dimensional model in the optically thin limit, and to the Beer-Lambert law for transmission attenuation.

One-dimensional Model

We consider an optically transparent rectangular duct exposed to collimated radiation through one of the walls as in the experiment. We assume the number density of particles to be known and uniform in space, the volume fraction to be small, and that particles and gas move together at the bulk velocity. Turbulent fluctuations are neglected. An energy balance on a differential control volume gives the system of coupled ordinary differential equations for the fluid and particle temperature rise shown in equations (1)-(2).

$$\rho_f c_{p,f} U \frac{dT_f}{dx} = n h_p A_p (T_p - T_f) \quad (1)$$

$$\rho_p c_{p,p} V_p U \frac{dT_p}{dx} = -h_p A_p (T_p - T_f) + \sigma_{abs} A_{pc} I \quad (2)$$

Here x and y denote the streamwise and wall-normal directions respectively, while the subscripts f and p refer to the fluid and particle phases. Density is designed by ρ, c_p is the specific heat, U is the bulk velocity, T is temperature, n is the particle number density, h_p is the particle to gas convective heat transfer coefficient, σ_{abs} is the absorption coefficient of radiation, and I is the radiation intensity seen by a particle. A_p, V_p and A_{pc} are particle geometrical parameters referring to the surface area, volume and projected cross-sectional area respectively. Note that by neglecting turbulent and diffusive transport, equations (1)-(2) are also valid if variables change in the wall normal direction, giving a quasi one-dimensional model (e.g. U(y), n(y), T(y), I(y)).

We define the following non-dimensional variables in analogy with conventional analysis of heat transfer in a pipe flow:

$$T^* = \frac{T - T_o}{T_o} \; ; \; x^* = \frac{x}{HRePr} \; ; \; I^* = RePr \frac{H}{L} \frac{\tau_{flow}}{\tau_{rad}} \frac{I}{I_o}$$

$$\gamma = RePr \frac{H}{L} \frac{\tau_{flow}}{\tau_{p,t}} \frac{c_{p,p}}{c_{p,f}} \; ; \; \beta = \gamma \left(\Phi + \frac{c_{p,f}}{c_{p,p}} \right)$$

T_o is the incoming temperature before the heated section of length L, $\tau_{flow} = L/U$ is the flow through time, $\tau_{p,t} = \left(\rho_p c_{p,p} V_p\right) / \left(h_p A_p\right)$is the particle thermal time constant, and $\tau_{rad} = \left(\rho_p c_{p,p} V_p T_o\right) / \left(\sigma_{abs} A_{pc} I_o\right)$ is the time for radiation to approximately double the initial particle temperature. No assumption has been made on the attenuation of the radiation intensity. In the so-called optically thin limit, the intensity is assumed constant across the domain and equal to the incoming radiation intensity I_o. This approximation holds for very low particle volume loadings. As the loading increases, particles deeper into the medium experience lower radiation intensity due to attenuation by particles located closer to the source. The previous system of equations has the following solution in the heated section in non-dimensional form:

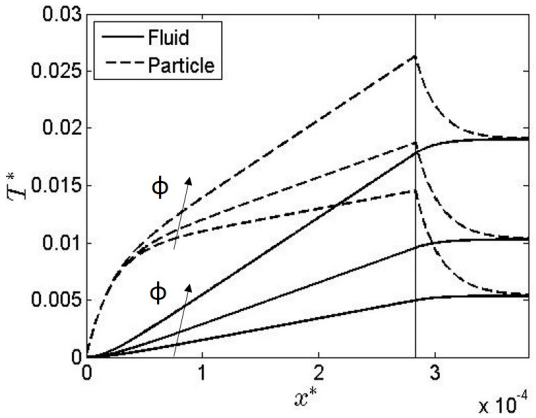

Figure 3. Evolution of non-dimensional particle and fluid temperature in the streamwise direction at $\Phi = 0.1$, 0.2, and 0.4. The vertical line denotes the end of the heated section.

$$T_p^* - T_f^* = \beta^{-1} I^* \left(1 - e^{-\beta x^*}\right) \quad (3)$$

$$T_f^* = \frac{\Phi}{\Phi + c_{p,f}/c_{p,p}} I^* x^* - \frac{\Phi}{\Phi + c_{p,f}/c_{p,p}} \beta^{-1} I^* \left(1 - e^{-\beta x^*}\right) \quad (4)$$

In the presence of turbulent fluctuations, this solution can be interpreted in terms of phase averaged temperatures in the wall normal direction (or mixed mean temperatures), and the solutions would be exact if turbulent correlations can be neglected.

The solutions show that after a short development length the particles and fluid achieve a constant temperature difference (eq.3), and the temperature of both phases then increases linearly in the streamwise direction. This regime can be considered thermally fully-developed in analogy with the thermally developed state in pipe flows with constant wall heat flux. Equation 4 reflects different regimes for the dependence of the rate of fluid temperature rise with mass loading. After the initial transient: $dT_f^*/dx^* \sim \Phi/(\Phi + c_{p,f}/c_{p,p})$. The fluid temperature rise rate is approximately linear with loading for small Φ, it is non linear as Φ becomes of $O(1)$, and at even larger loadings the rate of temperature increase saturates. Equation 3 indicates through the dependence of β on loading, that this saturation occurs in the model because the particle-fluid temperature difference decreases with increasing loading. It should be noted that for loadings greater than $O(1)$ additional effects such as two-way coupling, particle collisions, and other processes neglected in the model are expected to be important, and the model may be inaccurate.

The particle and fluid temperature solutions evaluated at the center of the duct for the experimental conditions and for the three mass loadings tested are shown in Fig. 3. The temperature solutions are extended to the streamwise location where the gas temperatures are measured, 55 mm downstream of the heated section. The same set of equations is solved in this region but without the radiative source term and using as initial conditions the fluid and particle temperatures at the end of the heated section. In the absence of external radiation the particle temperature decrease noticeable while the gas exhibits a marginal increase during this transient. The particle and fluid temperatures are nearly equilibrated at the measurement location.

We can use this one-dimensional model to compare the particle-solar receiver concept described in the introduction to a

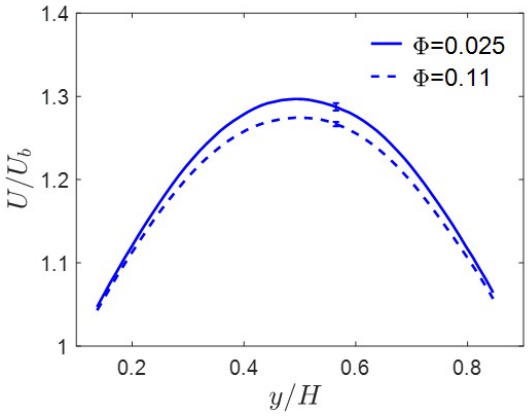

Figure 4. Mean streamwise particle velocity along the wall bisector for two mass loading ratios.

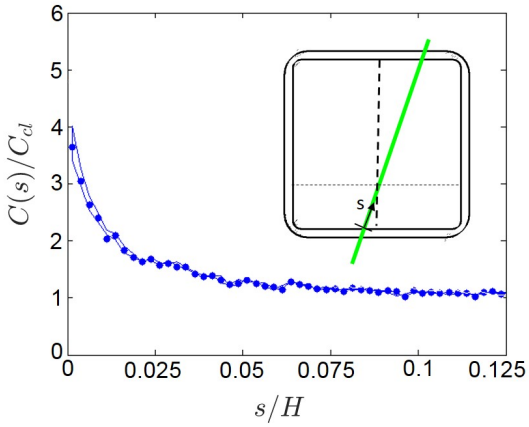

Figure 5. Mean particle concentration distribution along an inclined plane near the wall. The concentration is normalized by the value at the intersection with the wall bisector. $\Phi < 0.01$.

conventional solar receiver in which the heat transfer to the working fluid is provided by absorbing walls heated by solar radiation. One possible approach is to define the equivalent Nusselt number that would be required in the conventional system to provide the same fluid temperature rise but from four walls that are at the same temperature as the particles in the particle-solar receiver. Considering the fully-developed thermal state and substituting variables, the expression for the equivalent Nusselt number is given in equation 5. Using the experimental values, a $\mathrm{Nu}_{\mathrm{equiv}} \approx 450$ is required to obtain the same heat flux as in the experiments for $\Phi = 0.1$. For comparison, the Nusselt number for thermally fully developed turbulent pipe flow in air at a Reynolds number of $\mathrm{Re} = 20{,}000$ is $\mathrm{Nu} \approx 50$, which indicates that a much higher wall temperature would be required in a conventional solar receiver to achieve the heat flux provided by a particle-solar receiver.

$$\mathrm{Nu}_{\mathrm{equiv}} \equiv \frac{H}{k_f}\frac{q''}{T_p - T_f} = \frac{1}{4}\gamma \cdot \Phi \approx 4.5x10^3 \cdot \Phi \qquad (5)$$

Unheated Conditions

It is evident that the heat transfer from particles to gas and the gas temperature rise are affected by the particle number density and by the particle and fluid velocities. Therefore, variations of mean particle concentration and velocity across the test section yield non-uniform gas temperature rises. To analyze the effect of radiation absorption through measurements of the gas temperature rise, it is essential to have measurements of the particle concentration and velocity distributions. The experimental characterization of the particle phase was performed in the absence of heating to provide the inlet conditions to the radiated section. For the mild temperature rises considered to date, the mean particle motion can be considered unaltered in the presence of radiation.

We used two-dimensional PIV techniques to measure mean particle streamwise velocities at the central plane of the test section. The unladen gas velocities were measured using hot-wire anemometry. For the small time constant of the particles used in the experiments the particle to gas slip velocity is smaller than the uncertainty on the particle velocity measurements. Therefore, mean particles and gas velocities are assumed to be equal. Profiles of mean streamwise particle velocities along the wall bisector are shown in Fig. 4 for two mass loadings. Near-wall velocity measurements are not possible due to the test section corner radii. Mean velocities are higher than the bulk velocity in the central 75% of the test section width covered by the camera field of view. This velocity variation translates into different particle residence times in the radiated section, and implies a wall normal variation in the mean gas temperature profiles. The effect of increasing mass loading on the mean velocity is measurable but small (maximum differences <2%) for the two loadings shown in Fig. 4.

Variations of mean particle concentration affect the spatial temperature distribution through the dependence of the fluid temperature on the particle number density, and also have an important effect on the radiation attenuation. In the present experiments, the mean concentration was found to be uniform across most of the duct except in a small region near the walls due to turbophoretic effects. In wall bounded particle-laden turbulent flows, gradients in the wall-normal fluctuating fluid velocity are known to cause particles to drift towards the walls (Guha, 2008). The inclined laser sheet configuration shown in Fig. 2b was adopted to quantify the increase of concentration near the walls. Figure 5 shows the concentration profile measured for a mass loading ratio of less than 1%, along a 18 degrees inclined plane with respect to the wall normal direction. This low loading was required in order to accurately identify individual particles near the wall. Particle centroid coordinates identified over 2000 images were used to average the number of particles in 0.1 mm thick bins. Due to the inclined laser illumination and the finite thickness of the illumination sheet, particle concentrations are not experimentally accessible in the near wall region, under a y^+ of 1. The concentration drops quickly in a near wall region of less than 2.5% of the duct width (1 mm), and can be considered uniform in space beyond a region of about 7.5%. Therefore, in the bulk of the flow the number density of particles is uniform which justifies the assumption made in the one-dimensional model. It is important to notice that as the particle mass loading is increased in the experiments, inter-particle collisions become more important and are likely to reduce the relative increase of particle concentration near the wall. Therefore, the mean concentration becomes more uniform for increasing loadings.

Radiation Transmission

The total transmitted radiation through the particle-gas mixture is inferred from measurements of the radiation power incident on the calorimeter. The attenuation caused by the borosilicate walls as the radiation travels from the diode array to the calorimeter, was accounted for by measuring the transmitted radiation with particles and then immediately after without particles in the flow. The ratio

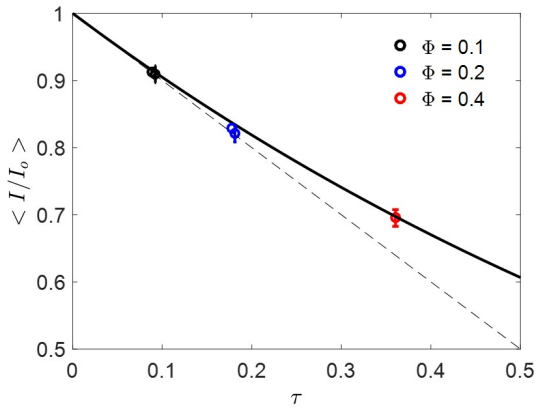

Figure 6. Total transmitted radiation as a function of optical depth. Symbols are experimental data. Repeated points indicate repeated experiments. The solid line is the Beer-Lambert law $I/I_o = e^{-\tau}$, and the light dashed line is the optically thin approximation $I/I_o = 1-\tau$.

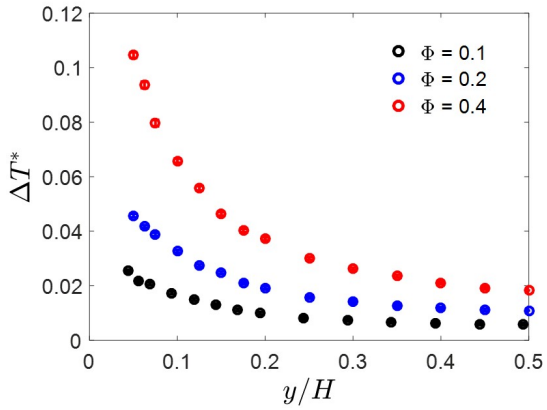

Figure 7. Non-dimensional temperature rise due to particles. Gas temperatures with and without particles in the flow are subtracted and divided by the unheated inlet temperature.

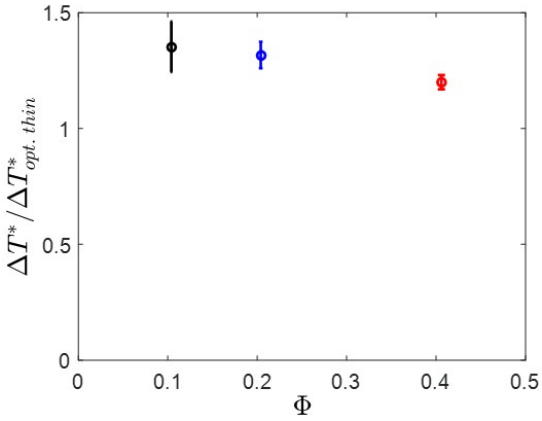

Figure 8. Non-dimensional temperature at the duct centerline, normalized by the one-dimensional optically thin model prediction.

of these two measurements cancels the effect of the glass attenuation. This ratio was used to compute the transmission loss due to particles only, which is equal to the total average intensity attenuation represented in Fig. 6 for the three mass loading ratios tested. Attenuation is plotted in terms of the optical depth, $\tau = \sigma_{ext} A_{pc} nH$, which was estimated assuming a uniform particle concentration to relate the mass loading ratio and number density. Therefore, τ is proportional to Φ. The extinction coefficient accounts for extinction due to absorption and scattering and it is obtained from tabulated values using the complex index of refraction from Mie scattering calculations.

The solid line in Fig. 6 represents the exponential decay of transmitted radiation through a medium with optical depth τ predicted by the Beer-Lambert law (Matsuda *et al.*, 2012). To within experimental error, and considering that the number density is not known exactly and that there is uncertainty in the the extinction coefficient, the data show good agreement with Beer-Lambert law. This indicates that the presence of preferential concentration in the experiments is not showing a large effect on the transmitted radiation. If the medium was optically thin, each particle would be exposed to the same radiative heat flux and the total transmitted power normalized by the irradiated area would obey the linear decay shown by the dashed line. The two lowest loadings are reasonably approximated by the optically thin assumption, while deviations are clear at $\Phi = 0.4$.

Gas Temperature Rise

Mean gas temperatures were measured along the wall bisector parallel to the beam path across the half of the test section width closest to the diode array. Radiation absorption by the walls adds further complexity in real wall bounded applications since the gas temperature rise is also affected by wall-to-fluid heat transfer. In order to evaluate the temperature rise caused only by the particles, temperature profiles were measured with and without particles and subtracted. In reality the system is not perfectly linear in this sense because particles may modify the turbulent transport of heat (Kuerten *et al.*, 2011), and so this decomposition is approximate.

Figure 7 plots the ratio of the temperature rise due to particles to the inlet temperature for the three mass loadings tested. The gas temperature rise increases with increasing mass loading as expected. Also, the temperature rise increases towards the wall due to the lower particle velocities as the particles are exposed to radiation for a longer time. Note that the gas temperature profiles shown correspond to the region where the particle concentration was measured to be uniform. Subtracting the inlet temperature from the gas temperatures in the presence of particles provides the total gas heating due to particles and wall heat transfer (results not shown for brevity). The ratio of the total gas temperature rise to the unheated gas temperature can be interpreted as a Boussinesq parameter. At the highest loading this quantity reaches values about 0.12 near the wall, providing an indication that buoyancy coupling may become important in the turbulent boundary layer.

The accuracy of the one-dimensional model using the optically thin assumption is examined in Fig. 8, which plots the gas temperature rise at the centerline of the duct normalized by the model prediction. In this particular case, the velocity used in the model is the measured centerline velocity of the particles. The fact that the values are greater than unity is artificial and is due to the peaked profile of the incident radiation across the duct width. The radiation beam profile is peaked at the wall bisector resulting in a higher incident flux at the central plane of the duct compared to the mean value across the full width. This does not prevent an analysis of the effect of increasing mass loading because the optically thin model is linear in the input radiation intensity. The normalized temperature difference decreases with mass loadings, in agreement with the radiation transmission results. At higher loadings particles become partially shadowed and experience less radiative flux at the centerline of the

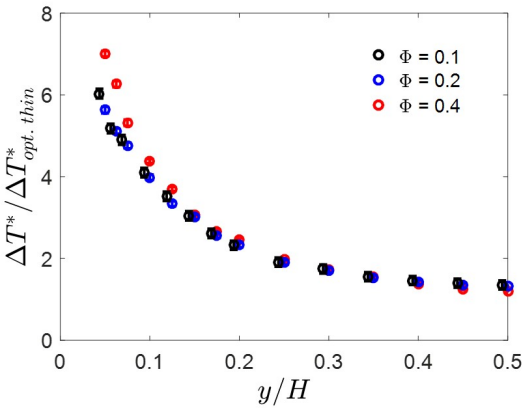

Figure 9. Non-dimensional temperature rise due to particles normalized by the one-dimensional optically thin model prediction at the duct center.

duct, resulting in reduced temperatures.

Figure 9 uses this same optically thin temperature rise at the center of the channel to rescale the profiles of gas temperature rise caused by the particles. Overall, the profiles are reasonably collapsed by the optically thin scaling reflecting that for the mass loadings analyzed the effects of decreased optical depth are not yet significantly large. For higher loadings, the quasi one-dimensional form of the model could be used to estimate the effect of varying optical depth along the temperature profile.

CONCLUSIONS

Radiation absorption by disperse, inertial particles in a turbulent square duct flow was examined experimentally and the results were compared to the predictions of a one-dimensional model assuming an optically thin medium. It was found that while the optically thin scaling accounts for most of the variation in temperature rise as a function of mass loading ratio, small deviations due to optical depth start to become apparent at the highest loading. Also, despite the presence of preferential concentration, transmission results were in good agreement with the exponential decay predicted by the Beer-Lambert law for a uniform absorbing medium. Future work will examine the effect of preferential concentration by measuring temporal fluctuations in the transmitted radiation and gas temperature.

REFERENCES

Bertocchi, R., Karni, J. & Kribus, A. 2004 Experimental evaluation of a non-isothermal high temperature solar particle receiver. *Energy* **29** (56), 687 – 700.

Brian, P.L.T., Hales, H.B. & Sherwood, T.K. 1969 Transport of heat and mass between liquids and spherical particles in an agitated tank. *AIChE Journal* **15**, 727–733.

Chen, H., Chen, Y., Hsieh, H.T. & Siegel, N. 2007 Computational fluid dynamics modeling of gas-particle flow within a solid-particle solar receiver. *Journal of solar energy engineering* **129** (2), 160–170.

Crocker, A. & Miller, F. 2011 Coupled fluid flow and radiative modeling for a small particle solar receiver. In *9th Annual International Energy Conversion Engineering Conference*, p. 5902.

Fessler, J.R., Kulick, J.D. & Eaton, J.K. 1994 Preferential concentration of heavy particles in a turbulent channel flow. *Physics of Fluids* **6** (11), 3742–3749.

Guha, A. 2008 Transport and deposition of particles in turbulent and laminar flow. *Annu. Rev. Fluid Mech.* **40**, 11–41.

Kim, K., Siegel, N., Kolb, G., Rangaswamy, V. & S.F, Moujaes 2009 A study of solid particle flow characterization in solar particle receiver. *Solar Energy* **83** (10), 1784 – 1793.

Klein, H.H., Rubin, R. & Karni, J. 2008 Experimental evaluation of particle consumption in a particle seeded solar receiver. *Journal of Solar Energy Engineering* **130**, 011012.

Kuerten, J.G.M, van der Geld, C.W.M. & Geurts, B.J. 2011 Turbulence modification and heat transfer enhancement by inertial particles in turbulent channel flow. *Phys. Fluids* **23**, 123301–8.

Lau, T.C.W. & Nathan, G.J. 2014 Influence of stokes number on the velocity and concentration distributions in particle-laden jets. *J. Fluid Mech.* **757**, 432–457.

Lenert, A. & Wang, E.N. 2012 Optimization of nanofluid volumetric receivers for solar thermal energy conversion. *Solar Energy* **86**, 253–265.

Matsuda, K., Onishi, R., Hirahara, M., Kurose, R., Takahashi, K. & Komori, S. 2014 Influence of microscale turbulent droplet clustering on radar cloud observations. *Journal of the Atmospheric Sciences* **71**, 3569–3581.

Matsuda, K., Onishi, R., Kurose, R. & Komori, S. 2012 Turbulence effect on cloud radiation. *Phys. Rev. Letters* **108**, 224502.

Maxey, M.R. 1987 The gravitational settling of aerosol particles in homogeneous turbulence and randow flow fields. *J. Fluid Mech.* **174**, 441–465.

Miller, F.J. & Koenigsdorff, R.W. 2000 Thermal modeling of a small-particle solar central receiver. *Journal of solar energy engineering* **122** (1), 23–29.

Pouransari, H. & Mani, A. 2017 Effects of preferential concentration on heat transfer in particle-based solar receivers. *Journal of Solar Energy Engineering* **139**, 021008–1–11.

Rahmani, M., Geraci, G., Iaccarino, G. & Mani, A. 2015 Polydisperse particles in an irradiated turbulent gas-particle mixture. *Center for Turbulence Research Annual Research Briefs* .

Reeks, M.W. 1983 The transport of discrete particles in inhomogeneous turbulence. *Journal of aerosol science* **14** (6), 729–739.

Shaw, R.A., Kostinski, A.B. & Lanterman, D.D. 2002 Super-exponential extinction of radiation in a negatively correlated random medium. *JQSRT* **75**, 13–20.

Squires, K.D. & Eaton, J.K. 1991 Preferential concentration of particles by turbulence. *Phys. Fluids A* **3**, 1169–1179.

Sundaram, S. & Collins, L.R. 1997 Collision statistics in an isotropic particle-laden turbulent suspension. part 1. direct numerical simulation. *J. Fluid Mech.* **335**, 75–109.

Villafañe, L., Banko, A.J., Elkins, C.J. & Eaton, J.K. 2017 *In Preparation* .

Villafañe, L., Moghadam, M.E., Banko, A. & Eaton, J.K. 2016 A robust method for quantification of preferential concentration from finite number of particles. *Center for Turbulence Research Annual Research Briefs* .

Williams, F.A. 1958 Spray combustion and atomization. *Phys. Fluids* **1**, 541–545.

Yapa, S.D., Elkins, C.J. & Eaton, J.K. 2015 Quantitative mri measurements of hot streak development in a turbine vane cascade. In *Proceedings of the ASME Turbo Expo*, , vol. 5B, pp. V05BT12A021–1–11. Montreal, Quebec, Canada.

Zamansky, R., Coletti, F., Massot, M. & Mani, A. 2014 Radiation induces turbulence in particle-laden flows. *Phys. Fluids* **26**, 071701.